NIST Technical Note
NIST TN 2247

An Automated System for Flow Characterization at Exhaust Ducts and Smokestacks

Rodney A. Bryant
Artur A. Chernovsky
Joseph A. Falco
Iosif I. Shinder

NIST | NATIONAL INSTITUTE OF STANDARDS AND TECHNOLOGY
U.S. DEPARTMENT OF COMMERCE

An Automated System for Flow Characterization at Exhaust Ducts and Smokestacks

Rodney A. Bryant
Artur A. Chernovsky
Fire Research Division
Engineering Laboratory

Joseph A. Falco
Intelligent Systems Division
Engineering Laboratory

Iosif I. Shinder
Sensor Science Division
Physical Measurement Laboratory

NIST TN 2247
February 2023

Certain commercial entities, equipment, or materials may be identified in this document in order to describe an experimental procedure or concept adequately. Such identification is not intended to imply recommendation or endorsement by the National Institute of Standards and Technology, nor is it intended to imply that the entities, materials, or equipment are necessarily the best available for the purpose.

NIST Technical Series Policies

Publication History
Approved by the NIST Editorial Review Board on 2023-02-07

How to Cite this NIST Technical Series Publication

NIST Author ORCID iDs
Rodney A. Bryant: 0000-0002-5344-9878
Artur A. Chernovsky: 0000-0002-1215-7350
Joseph A. Falco: 0000-0002-7794-5331
Iosif I. Shinder: 0000-0001-7994-6699

.

Abstract

This report summarizes the design and description for an automated system of velocity traverse probes. Performance of key components of the system are also described. The system is designed for conducting detailed characterizations of flow distributions in exhaust ducts and smokestacks. Accurate flow measurements in large exhaust systems for flue gases are critical for quantifying greenhouse gas and pollutant emissions due to fossil fuel combustion. Field deployment of the system has been demonstrated. It will be utilized to conduct in-line calibrations of the flow monitoring devices installed at the exhaust ducts of the National Fire Research Laboratory. The system is a prototype for future designs which can be applied to characterize flow conditions for similarly-sized exhaust ducts and smokestacks. Other potential uses of the system are for precise positioning of probes and instruments in and around adverse environments such as enclosure fires or open burns.

Keywords

Table of Contents

List of Tables

List of Figures

Acknowledgments

1.   Introduction

Emission rates of greenhouse gases and pollutants from the smokestacks of stationary sources are determined by measuring pollutant concentration and total flow. Therefore, accurate flow measurements in flue gas exhaust systems are critical for quantifying emissions from fossil fuel combustion. The National Fire Research Laboratory (NFRL), a National Institute of Standards and Technology (NIST) research facility for the development of better fire safety performance of buildings, routinely monitors and controls flue gas emissions when conducting large-scale fire experiments. Accurate measurements of emission rates are necessary to compute parameters key to evaluating fire safety. The measurement capabilities of the NFRL are being utilized to demonstrate best practices for accurate measurements of total flow in exhaust ducts and smokestacks.

Using existing test methods, detailed flow characterizations were initially conducted by manually "pushing" and "pulling" velocity probes across the NFRL exhaust ducts. [1] Because the experiments were labor intensive, only a limited set of conditions were studied. Subsequently, a major expansion of the NFRL occurred that included the installation of a 20 MW calorimeter. [2] The expansion increased the size and number of exhaust ducts, and therefore increased the range of flow conditions to characterize. Hence, an automated system was built to improve efficiency in the campaign to characterize the exhaust flows while also improving measurement accuracy.

This report provides the design and technical description of the automated traverse probe system and summarizes the results of its performance evaluations. Ultimately the system will be utilized to conduct in-line calibrations for the NFRL's routine flow monitoring devices using standard test methods of the emissions industry for determining the accuracy of flow monitoring systems installed at exhaust ducts and smokestacks for continuous emissions monitoring.

1.1.   Standard Test Methods for Flow Characterization

Continuous emissions monitoring systems (CEMS) are integrated instruments permanently installed at a smokestack or flue-gas exhaust system to continuously measure volumetric flow and pollutant concentration, Fig. 1. These systems are required to monitor the emissions for regulated pollutants and greenhouse gases. Regulatory agencies such as the U.S. Environmental Protection Agency (EPA) require periodic audits of CEMS using reference standards or test methods to evaluate the accuracy of emissions reporting. Test methods, such as EPA Method 2G (40 CFR Part 60), ASTM D3154, and ISO 10780, exist for determining average velocity in ducts, stacks, or flue pipes using pitot type probes. [3-5] These are reference test methods that provide a detailed set of procedures for in-line calibrations of CEMS flow monitoring devices.

For a flow audit, certified auditors will temporarily install measurement equipment on the smokestack or exhaust duct and follow the procedures of the reference test methods to measure average velocity and volume flow. It is typical that someone manually "pushes" and "pulls" a velocity probe across the exhaust duct or smokestack to conduct the flow audit. EPA Method 2G recognizes that technology for automating many of the procedures of the flow audit exists and allows for its use. [3] Several flow auditing companies use automated systems for CEMS audits and hold patents for the technology.[6-8]
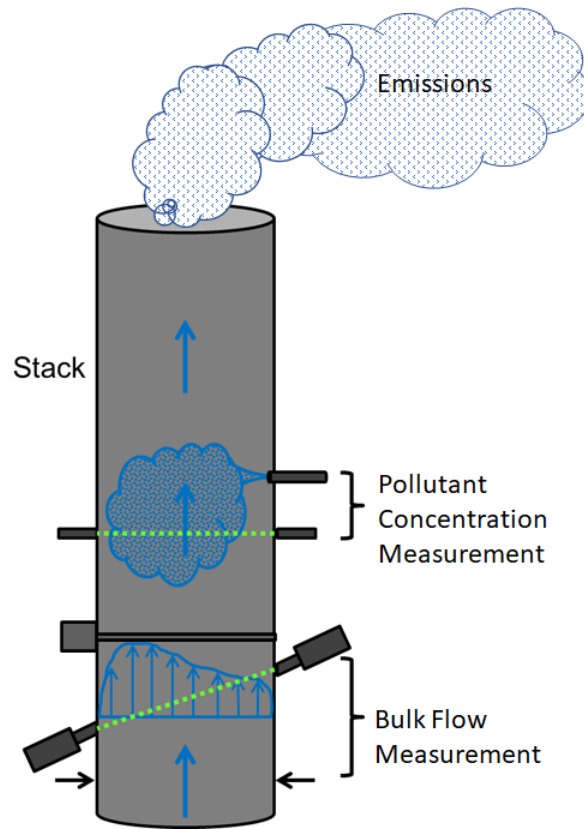
Fig. 1. Diagram of generic CEMS installation at a smokestack.
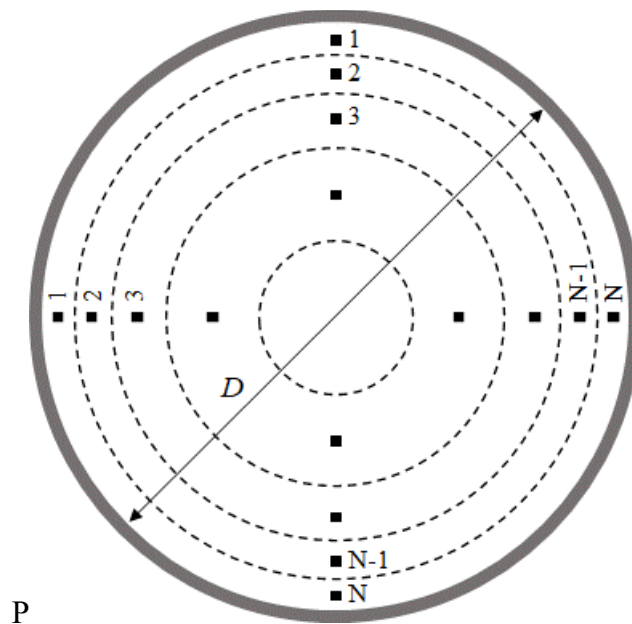
Fig. 2. Traverse positions for centroid of equal areas.

2

The procedures specify the use of pitot type probes to measure gas velocity at discrete points. For combustion gases or particulate and droplet laden flows, the "S-Probe", a special pitot probe with two large and symmetric openings, is used most often as it is not easily clogged (see Fig. 5). The S-probes are traversed along two orthogonal chords as shown in Fig. 2 and velocity is measured at prescribed locations as listed in Table 1. Measurement locations are determined according to the size of the duct and the number of measurements. For circular cross sections, measurements are located at the center of annular regions of equal area (centroid of equal areas), Fig. 2. Since each velocity measurement has equal weighting, the arithmetic average of the measurements determines the average velocity.

Table 1. Example traverse positions, *d/D*, for circular ducts (centroid of equal areas).

Traverse Point	6 Points on Diameter	12 Points on Diameter	24 Points on Diameter
1	0.044	0.021	0.011
2	0.146	0.067	0.032
3	0.296	0.118	0.055
4	0.704	0.177	0.079
5	0.854	0.250	0.105
6	0.956	0.356	0.132
7		0.644	0.161
8		0.750	0.194
9		0.823	0.230
10		0.882	0.272
11		0.933	0.323
12		0.979	0.398
13			0.602
14			0.677
15			0.728
16			0.770
17			0.806
18			0.839
19			0.868
20			0.895
21			0.921
22			0.945
23			0.968
24			0.989

2.   Conceptual Design

Past experiments to characterize the flow at the exhaust ducts of the NFRL provided the experience and knowledge to design an automated and remotely operated flow traverse system. From this experience a system meeting the following objectives was designed:

1) capable of determining yaw angle and near-axial velocity, at multiple traverse locations

2) capable of performing the functions and procedures of the reference test methods

3) remote and reliable operations and control

4) weatherproof for extended deployment

5) scripted automation

6) accurate results

Following the guidance of the design objectives, a list of fundamental requirements was developed to create a system capable of meeting or exceeding the recommended performance described in the reference test methods.

Fundamental Requirements:

1) Linear positioning of probe for a distance of 0 m to 2.5 m; accurate to ±0.003 m.

2) Rotational positioning of probe ranging from 0° to 270°; accurate to ±3.0°.

3) Probe shaft (linear rail) shall not bend or sag more than 5° from the intended chord path when fully extended.

4) Flow blockage from fully extend probe shaft shall be less than 4 %.

5) Electronics shall be operational between 5 °C and 40 °C.

6) Electronics shall be housed in weatherproof enclosures.

7) Probe shall maintain linear and rotational reference positions.

8) Limit switches or hard stops shall be used to prevent the probe from extending beyond it's intended range and causing damage to the probe and its surroundings.

9) Probe shall be mounted at standard ports (10.16 cm [4 in] nominal pipe size with ASME class 150 flange) on ducts and stacks.

10) System shall consist of modular components of manageable weight and size for deployment to elevated locations such as rooftops or smokestacks.

11) System shall receive and execute positioning commands from a remote source (network computer).

12) System shall execute manually entered commands.

13) System shall execute a scripted set of commands.

14) System shall be capable of remote start, shutdown, and restart.

These fundamental requirements were expanded in detail to deliver accurate results while following the procedures described in the standards. Software was developed for remote operations as well as prescribed operations from a scripted set of commands. Fig. 3 shows the drawing used to fabricate a system based on the previous lists of objectives and requirements.
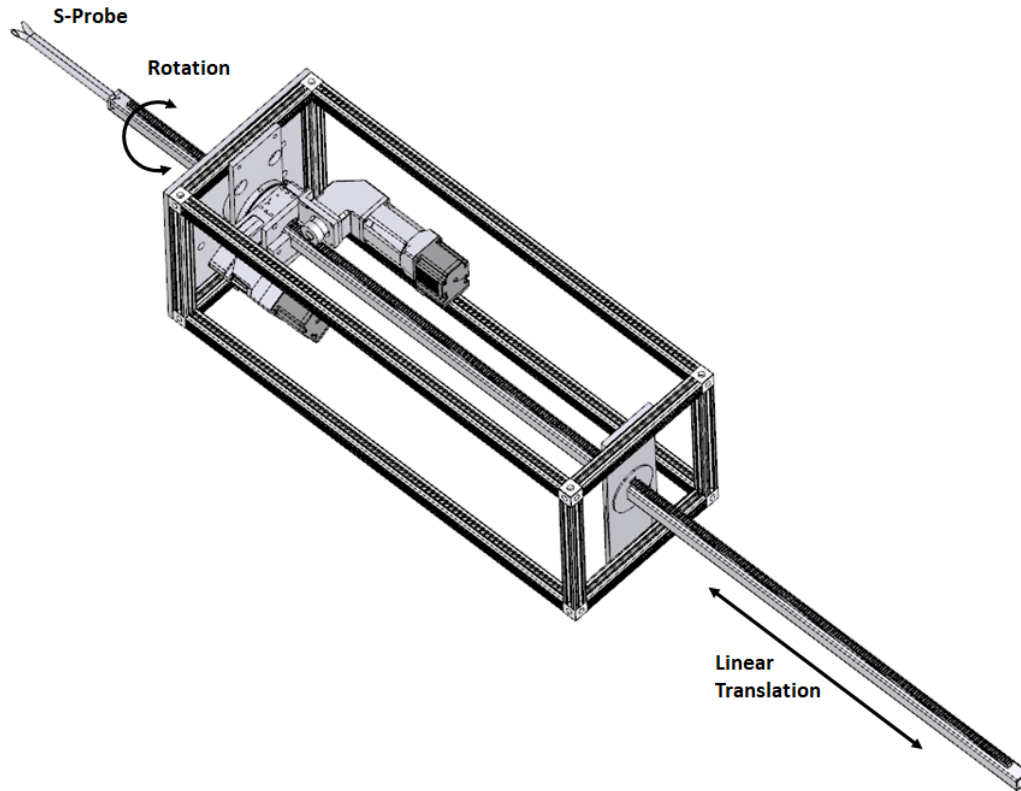
Fig. 3. Fabrication drawing for the automated traverse probe.

3.   Materials and Procedures

3.1.   Automated Traverse

The auto traverse system was developed by integrating two smartmotors (MOOG Animatics, Model SM23165DT) to provide precise linear and rotational positioning of the probe tip. Smartmotors are servomotors with controllers, amplifiers, and encoders integrated in a single motor package. For linear positioning, the smartmotor is coupled to a 22:1 right angle gearhead, which turns a spur gear to drive a linear rail (rack and pinion). The linear rail consists of a 20-pitch rack, mounted to a 2.54 cm (1 in) square tube. For rotational positioning the smartmotor is coupled to a 10:1 speed reducing gearhead, which turns a belt-driven rotational stage (Bell-Everman SBR50). The rotational stage has a 50 mm through hole to accommodate

mounting and passage of the linear rail. The linear traverse is mounted to the rotary traverse which is mounted to a rigid plate. The plate is attached to a frame of extruded aluminum for support of the linear rail and mounting to exhaust duct ports. Annotated photographs of the system are shown in Fig. 4.
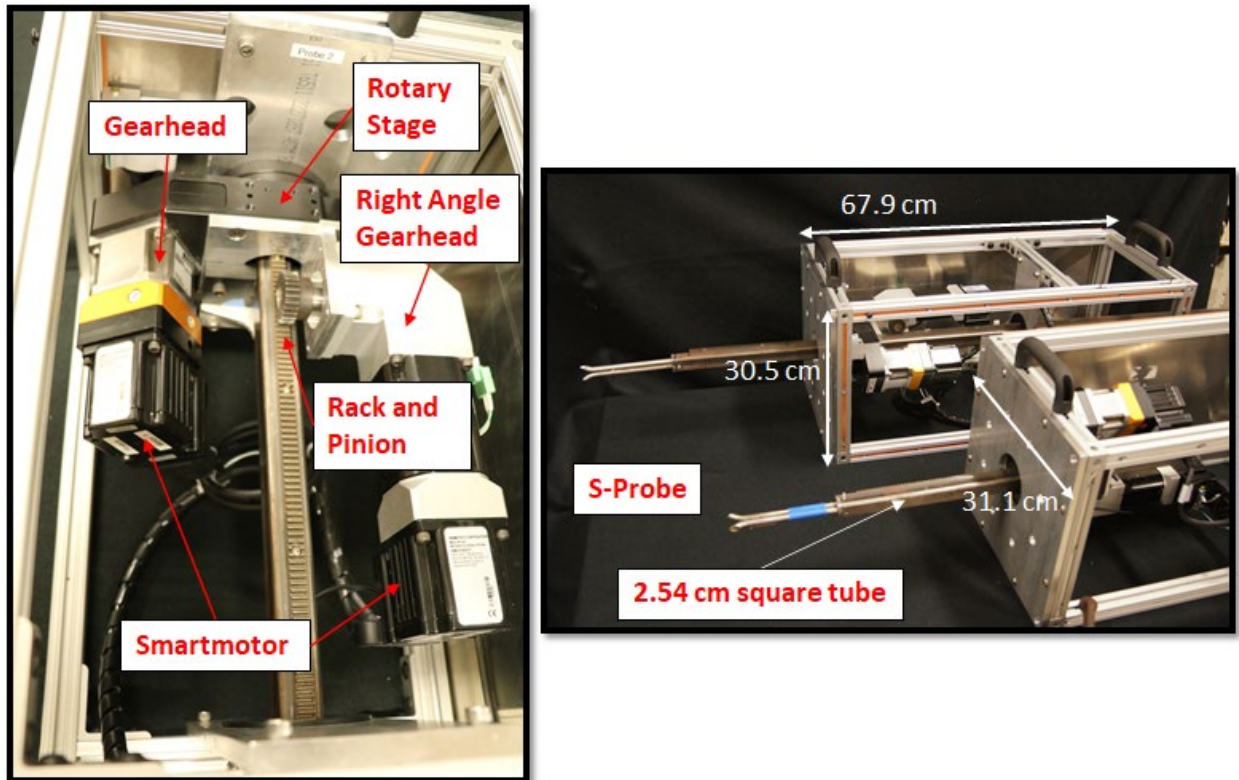
Fig. 4. Photographs of automated traverse probes.

3.2. Velocity Probes

S-probes (Environmental Supply Co., PPS12-Y-024) are mounted on the auto traverse system. They are made from 0.95 cm (3/8 in) stainless steel tubing and fabricated to the specifications defined in EPA Method 2. [9] The S-probe has large openings to prevent clogging from particulates and droplets. The probe is symmetric and can detect flow in either direction when paired with a bi-directional pressure transducer. The probes were modified with hose barb fittings and a mounting interface as shown in Fig. 5. The mounting interface allowed adjustment for the length of probe extended beyond the rail. Flexible pressure leads were fed through the hollow rail and attached to the hose barbs at the end of the probe. For this and subsequent investigations, the A-side of the probe faces upstream. It is first to receive the flow, and experiences stagnation pressure; while the B-side faces downstream and experiences a reduced pressure. A bare bead thermocouple (Omega Type K) is installed 2.54 cm from the tip of the pressure openings using fiberglass tape. Wiring for the thermocouple also passes through the square tube.
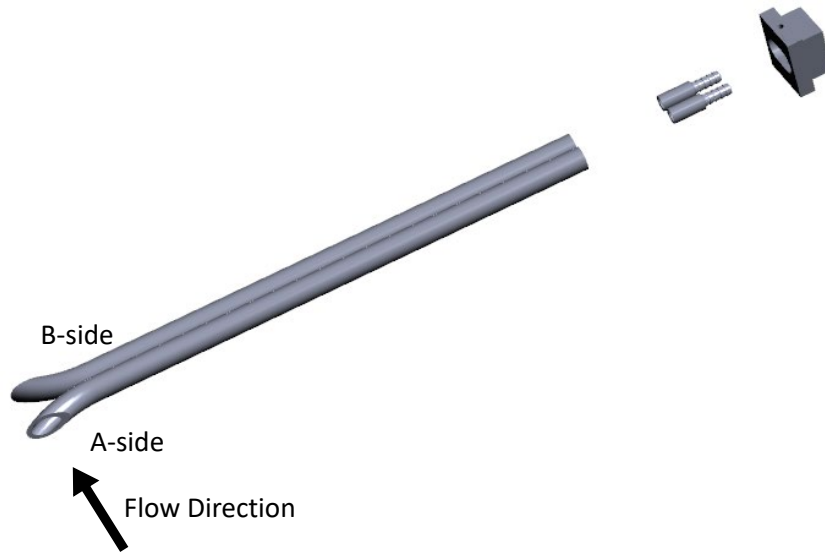
Fig. 5. Exploded-view diagram the of S-type pitot probe.

3.3. Instrumentation and Data Acquisition

The pressure differential, ΔP, induced by flow across the S-probe is measured with precision capacitance manometers (MKS 220D Baratron). Two manometers are attached to the leads of each probe, one having a range of 0 Pa to 133.32 Pa and the other having a range of 0 Pa to 1333.2 Pa. Both are calibrated against the NFRL's working standard for pressure (NFRL WSTD 577967), a high-accuracy capacitance manometer (MKS 698A Baratron). The relative expanded uncertainty[1] of the differential pressure measurement is estimated at 1.0 % for the low range transducers (133.32 Pa) and 0.6 % for the high range transducers (1333.2 Pa).

Density of the exhaust gas, ρ_e, is derived from the temperature measurement, T, at the probe using a bare-bead thermocouple (Omega Type K). The relative expanded uncertainty of the gas temperature measurement is estimated at 1.0 %. Static pressure in the exhaust duct, P_s, is measured with a digital barometer (Vaisala PTU303) with an expanded uncertainty of 15 Pa. The molecular mass, M_e, of the exhaust gas is assumed to be equal to that of dry ambient air, (28.97 ± 0.10) kg/kmol.

---

[1] Unless otherwise stated, all uncertainty values are reported as expanded uncertainty, for a 95% confidence interval with a coverage factor $k = 2.0$.
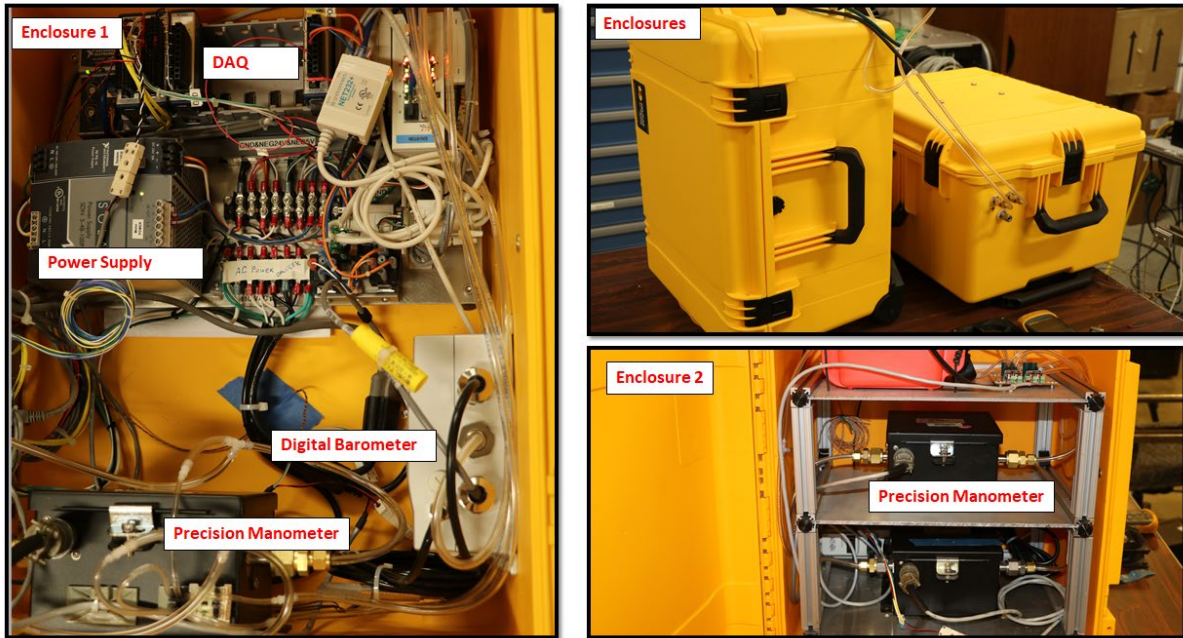
Fig. 6. Photographs of the enclosures containing instrumentation, data acquisition, and power management.

The instrumentation and electronics are contained in two weatherproof enclosures, Fig. 6. Data acquisition is performed using a networked data acquisition chassis (National Instruments cDAQ-9188XT) containing input/output modules for voltage, temperature, digital waveforms, and power relays. The digitized signals are scaled and logged using NFRL's custom data acquisition application, MIDAS. Serial commands and data are transmitted using RS-232 serial-to-ethernet communications modules. Electrical power for the smartmotors and other system components is provided by two AC/DC power supplies (SOLA SDN 5-48-100P 48 V, 240 W and National Instruments PS-15 24 V, 120 W). All data and commands are transmitted over the local area network. NFRL's custom data-sharing application, DataBridge, is utilized to share real-time data across multiple client applications.

3.4.   Remote Operation and Automation

User interface software is provided by the smartmotor manufacturer (MOOG Animatics) that allows the user to program the motor by setting parameters such as motor acceleration, speed, travel limits, etc. The code is stored to the motor's memory and sets the operational profile of the motor. A separate software application was developed to remotely operate the system and automate the procedures for conducting a flow survey as described by the standard test methods. Commands to power the motors on/off, move the probe to a desired location (jog or location value), or load a sequence of movements (script) to the software application are entered using the graphical user interface (GUI), shown in Fig. 7. The GUI also provides feedback for monitoring probe position, smartmotor status, and error handling. Additional popup windows, not shown

here, are available to provide data on smartmotor health, as well as real-time graphical data during the probe nulling routine.
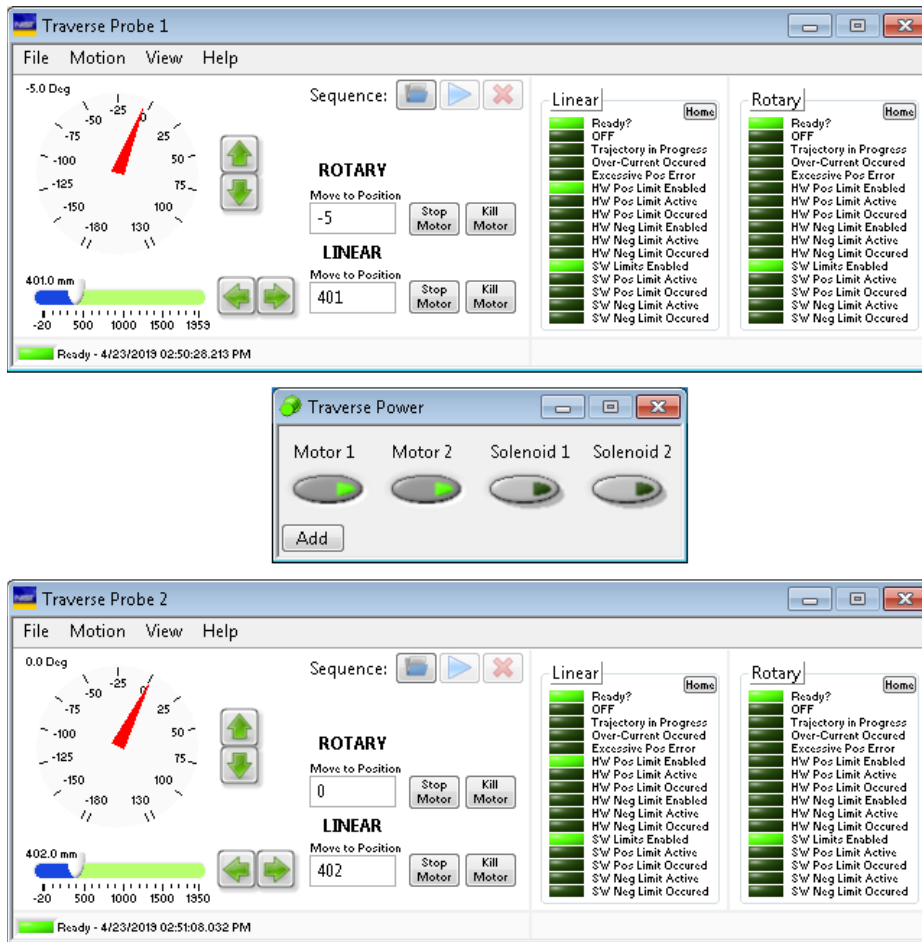
Fig. 7. Graphical user interface for operating the automated traverse probe.

The operational software is based on a modular architecture. Each module is self-contained and operates independently of other modules. The modules, Traverse Probe 1 and Traverse Probe 2, are shown in Fig. 7. If additional traverse probes are added, software modules can be duplicated and modified to incorporate the additional hardware.

The software modules provide motion control of the smartmotors either as a single command or a sequence of commands from a script file. Automation of the procedures for conducting a flow survey was achieved using script files. The flow survey procedures are summarized as follows:

1) Move probe to first linear traverse position, $d_{i=1}$, and rotate the probe to align with the duct axis, $\theta = 0.0°$.

2) Rotate probe and monitor differential pressure to determine null angle (θ_{null} at $\Delta P \cong 0.0$ Pa).

3) Rotate probe 90° ($\theta_y = \theta_{null} \pm 90°$) to align probe with flow and measure near axial velocity.

4) Record differential pressure ($\Delta P_{i=1}$), gas temperature ($T_{i=1}$), flow yaw angle ($\theta_{y,i=1}$), and linear position ($d_{i=1}$) of the probe; and static pressure in the exhaust duct ($P_{s,i=1}$).

5) Move probe to next traverse position, d_{i+1}; realign probe with the duct axis, $\theta = 0.0°$, and repeat Steps 2 – 4.

6) Repeat Step 5 until flow traverse is complete.

The script file passes arrays of commands in sequence for probe positioning, yaw angle determination, data tagging, etc., therefore instructing the motors to position the probe and execute the procedures summarized above.

4. Results – Performance Characterization

4.1. Linear Positioning

A tape measure was used as the reference measurement for converting encoder counts to linear distance in millimeters. The estimated accuracy of the tape measure is ±2.0 mm (includes operator error). A series of experiments were conducted to estimate the precision of the linear positioning system, for three mounting configurations – horizontal, horizontal-cantilevered, and vertical. Encoder counts for 13 repeat experiments are plotted in Fig. 8. The standard error of the linear least squares fit for encoder counts was ±408, which scales to an estimated precision of ±0.5 mm. Similar experiments using a tape measure to provide an independent measure of linear position estimated the precision at ±1.0 mm. The most conservative result for precision, ±1.0 mm, was used to estimate combined uncertainty. Adding the standard accuracy of the tape measure, ±2.0 mm/2, and the measured precision of the system, ±1.0 mm, in quadrature, the expanded uncertainty of the linear positioning for the automated traverse probe is estimated at ±3.0 mm. This meets the desired requirements, however it is possible to reduce the uncertainty by utilizing a reference measurement with higher accuracy, such as a laser distance meter.
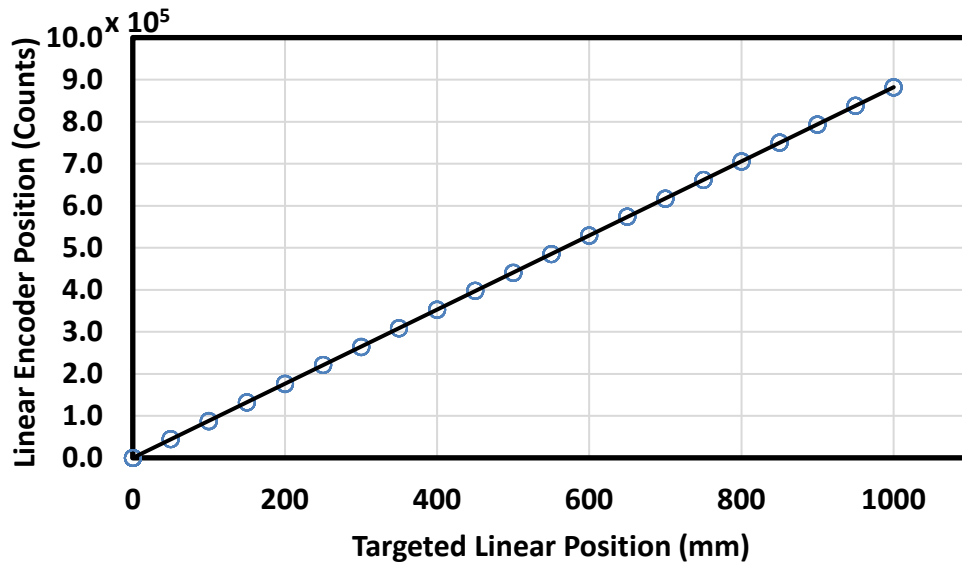
Fig. 8. Results of experiments to estimate the precision for linear positioning.

4.2. Rotational Positioning

A digital level with ±0.1° accuracy was used as the reference measurement for converting encoder counts to rotational position in degrees. Experiments to estimate the precision of the rotational positioning system were conducted with the digital level attached to the probe rail. Readings from the digital level and smartmotor encoder were recorded for 8 repeat experiments. The results from the digital level are shown in Fig. 9. The linear least squares fit of the digital level readings has a standard error of ±1.4°, while the fit for the encoder has a standard error of ±81 counts (scales to ±0.2°). Error due to play at the mount that transfers rotational motion to the rail is included in the readings from the digital level. Therefore, the standard error from the fit of data from the digital level is the appropriate measure to estimate precision of the rotational system. Adding the standard accuracy of the digital level, ±0.1°/2, and the precision of the rotational system, ±1.4°, in quadrature, the expanded uncertainty of rotational positioning for the automated traverse probe is estimated at ±2.8°. This meets the desired requirements; however it is possible to reduce this uncertainty by improving the mounting of the rail to the rotary stage and thereby reducing the resulting play in the transfer of rotational motion to the rail.

11
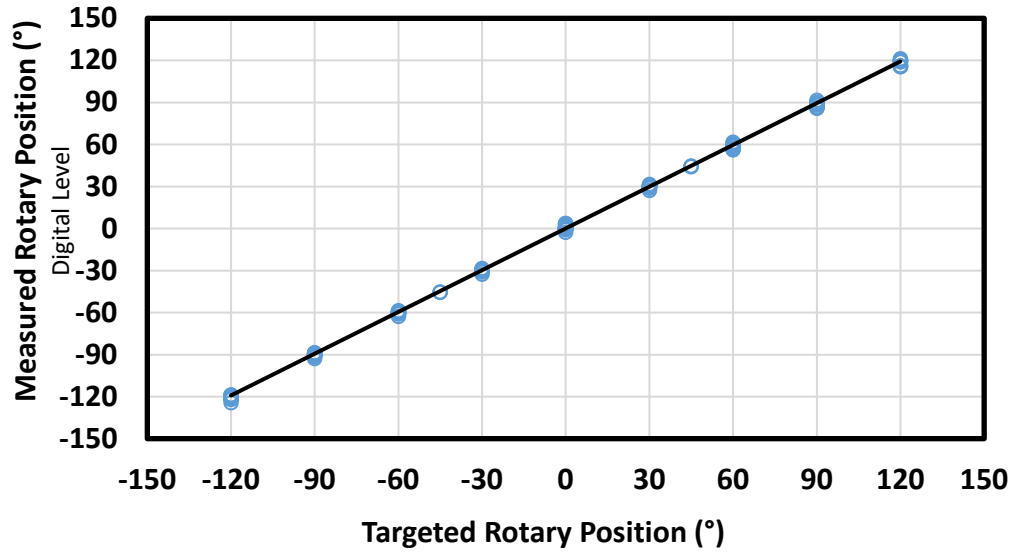
Fig. 9. Results of experiments to estimate the precision for rotational positioning.

4.3. S-Probe Calibration

Flow across an S-probe induces a pressure differential, ΔP, at the pressure ports. Local gas density, ρ_e, is derived using the temperature measurement, T, at the probe and the static pressure, P_s, in the duct. Yaw angle of the flow, θ_y, is the inclination of the flow relative to the axis of the stack or duct. These measurements are used to compute the near-axial velocity at the probe.

$$V_{SP} = C_{SP}\cos(\theta_y)\sqrt{2\Delta PT\frac{R}{P_s M_e}} \qquad (1)$$

The calibration coefficient, C_{SP}, can be determined using the calibration procedures described in EPA Method 2G [3] or it can be assigned a value of 0.84 when the dimensional parameters of the S-probe are compliant with EPA Method 2. [9] Previous experience has shown the calibration coefficient to be influenced by flow speed, with values ranging from 0.80 to 0.85. Therefore, each probe was calibrated in the NIST Airspeed Calibration Facility. [10] For this application, the calibration coefficients are represented as functions of the differential pressure measured at the S-probe. Power law fits, listed in Table 2, were derived from the calibration data and are used to compute calibration coefficients for each probe.

Calibrations were performed using the tertiary working standard – a pitot tube, traceable to the International System of units (SI). The relative expanded uncertainty of the working standard is estimated at 0.44 %. [11] The S-probes were rotated to align with the bulk flow, $\theta_y = 0.0°$, during calibration. Calibrations for S-probe 1401 were performed for wind tunnel flows with 0 % to 10 % turbulence intensity. The data is shown in Fig. 10 and the relative root mean square error (RMSE) of the fit is 1.27 %. Assuming the variation in the data is mostly due to the range of turbulent conditions, the uncertainty due to turbulence is estimated as the RMSE of the fit.

The relative RMSE of the calibration data for all three probes at 0 % turbulence is 0.71 %. This is less than 60 % of the observed RMSE at all conditions for S-probe 1401, and therefore this assumption is reasonable. Adding the standard uncertainty of the working standard, 0.44 %/2, and the uncertainty due to turbulence, 1.27 %, the expanded uncertainty of the calibration coefficients is estimated at ±2.6 %.
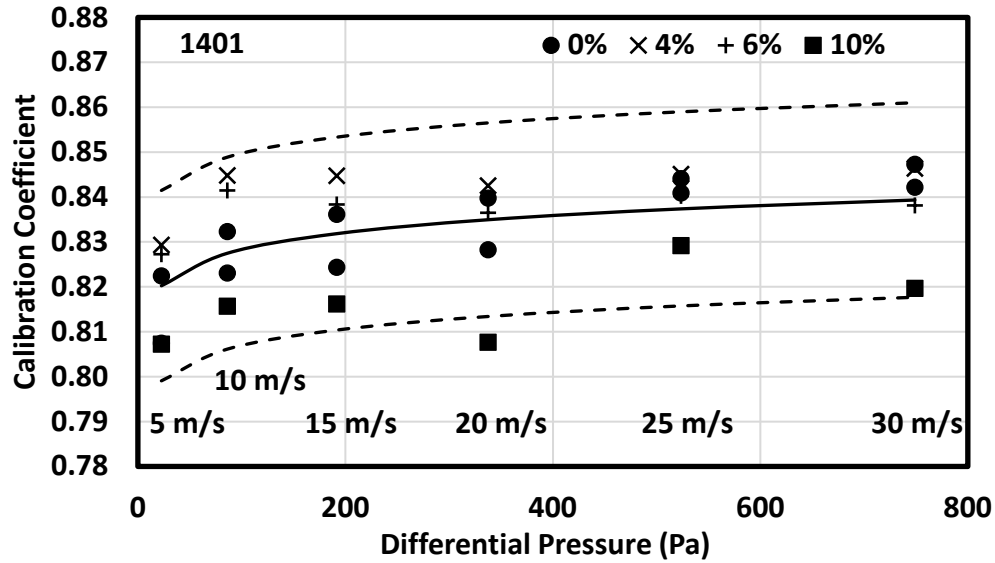
Fig. 10. Calibration results for S-probe 1401. Symbols represent the percentage of turbulence in the wind tunnel flow. The solid line represents a power law fit to the data; dashed lines represent expanded uncertainty. The flow speed is indicated below each grouping of symbols.

Table 2. Functions for computing S-Probe calibration coefficients.

Probe #	C_{SP}
1401	$0.8036\Delta P^{0.006576}$
1402	$0.7995\Delta P^{0.008514}$
1403	$0.8200\Delta P^{0.002175}$

4.4.   Yaw Angle Determination

Flow yaw angle is determined by nulling the S-probe, therefore rotating the probe until the differential pressure reads zero (null). Rotating the probe 90° back from the null position properly aligns the probe with the flow. Hence the flow or yaw angle is $\theta_y = \theta_{null} - 90°$ for a clockwise rotation as shown in Fig. 11. For a counter-clockwise rotation, $\theta_y = \theta_{null} + 90°$. A script was written to automate the yaw-nulling procedure. The probe rotated in steps of 5° and differential pressure was recorded at each step. Rotation started near the anticipated null position to ensure that the differential pressure passed through the zero, as shown in the "Nulling" regions in Fig. 12. The automation includes a linear interpolation of the data to determine the null angle. A pop-up window is available for the user to see the results of the linear interpolation in real-time (see insert graph in Fig. 14). Once the null angle was computed the probe rotated 90° in the opposite direction to align with the flow. Flow alignment is demonstrated in Fig. 12 as the period (700 s – 730 s) between the two nulling procedures where the rotational position of the probe is held constant.
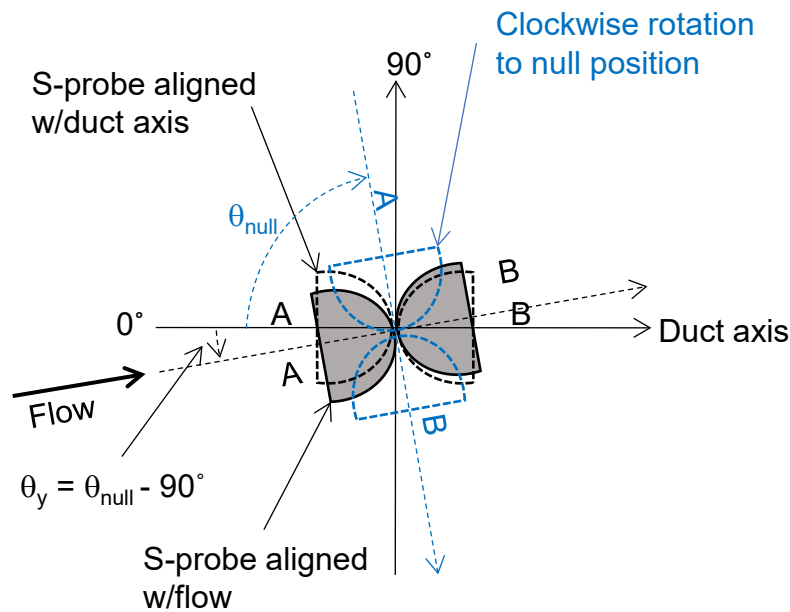
Fig. 11. S-probe orientation during the yaw-nulling procedure.
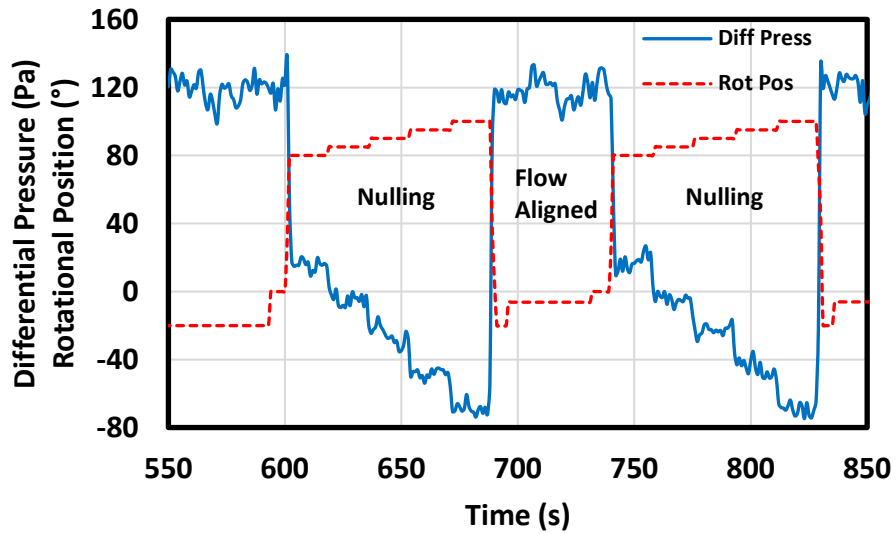
Fig. 12. Time trace of the yaw-nulling procedure. Differential pressure is plotted as the blue trace; rotational position of the S-probe is plotted as the red dashed trace.

The automated yaw-nulling procedure was developed and tested using an electric blower as shown in Fig. 13. The blower generated a wind field, and it was tilted to produce flow at an arbitrary angle relative to horizontal. The S-probe was positioned in the wind field and the nulling procedure was run to determine the flow angle. Optimization of the nulling procedure included adjusting the increments of rotation and periods of data averaging to reduce the null discrepancy when confirming the computed null position. Confirmation required rotating the probe back to the computed null position and measuring the differential pressure. The system was able to confirm null pressure within ±1.5 Pa.

Fig. 13. Photograph of electric blower. The blower provided a wind field for testing the yaw-nulling procedure using the S-probe.

Experiments were conducted to characterize how precise the system could determine flow yaw angle, θ_y. Using the setup shown in Fig. 13, the automated nulling procedure was repeated 60 times (30 with clockwise rotation, 30 with counter-clockwise rotation) for a single flow angle. Table 3 list the results from the experiments. The absolute difference of the means is 0.62° and is likely the result of error due to play in the mounting of the rail to the rotary stage. This difference is added in quadrature with the maximum standard deviation, 0.52°, to estimate the precision for determining flow yaw angle, ±0.8°. Adding the standard uncertainty for rotational positioning, ±2.8°/2, and the estimated precision, ±0.8°, in quadrature, the expanded uncertainty of the procedure to determine flow yaw angle is estimated at ±3.2°.

Table 3. Characterization of the yaw-nulling procedure.

Nulling Rotation	Yaw Angle, θ_y (°) mean $\pm \sigma$
Clockwise (impact port up at null)	-6.30 ± 0.35
Counter-Clockwise (impact port down at null)	-5.68 ± 0.52
Difference	$\lvert -0.62 \rvert$

4.5. Deployment Demonstration

The automated traverse system was deployed to the roof of the NFRL for demonstration and troubleshooting. The probes were mounted at ports on the exhaust duct to conduct flow traverses for two orthogonal chords at a cross section. Effective inner diameter of the exhaust duct is 1.975 m. Probe 1 traversed the horizontal chord while Probe 2 traversed the vertical chord. Network-based video cameras provided visual feedback of the probes during operations, Fig. 14. The video streams were captured and broadcast to local web pages using NFRL's custom video capture application.
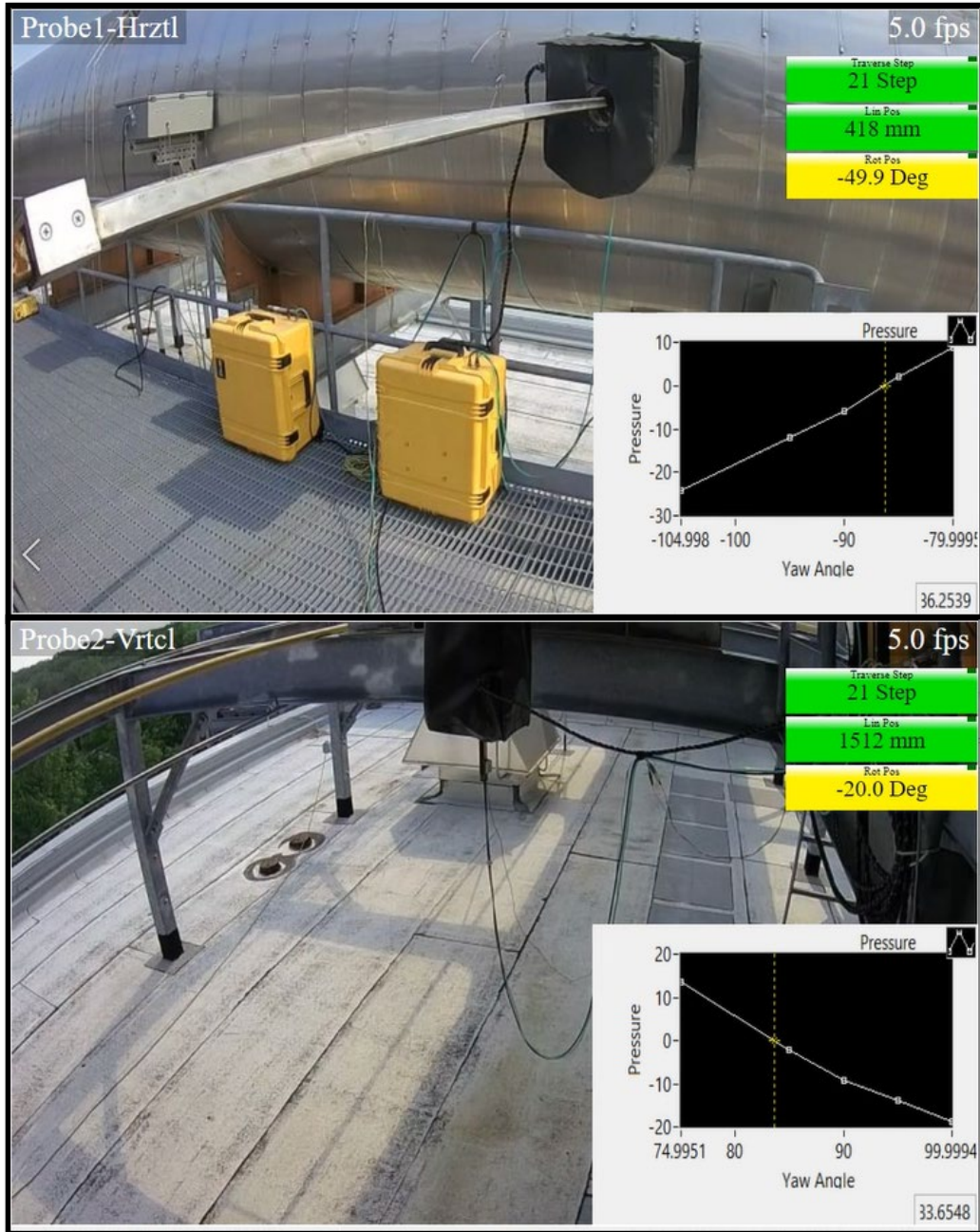
Fig. 14. Snapshots from video monitoring of automated traverse probes during a flow characterization experiment at the NFRL exhaust duct. Inset is graph of differential pressure plotted with respect to probe angle during the yaw-nulling procedure.

A script file was loaded at the user interface and initiated to conduct a 30-point traverse and measure the near axial velocity at each point. The yaw-nulling procedure was performed at each point to determine flow yaw angle, Fig. 15, and align the S-probe with the flow. For this demonstration, yaw angle ranged from -6.7° to 5.0° across the duct. The distributions of yaw angle were similar on both chords, with the exception of outliers near the inner wall of the

exhaust duct. Probe mounting ports are located at the inner wall and air leakage at the ports can influence the flow.
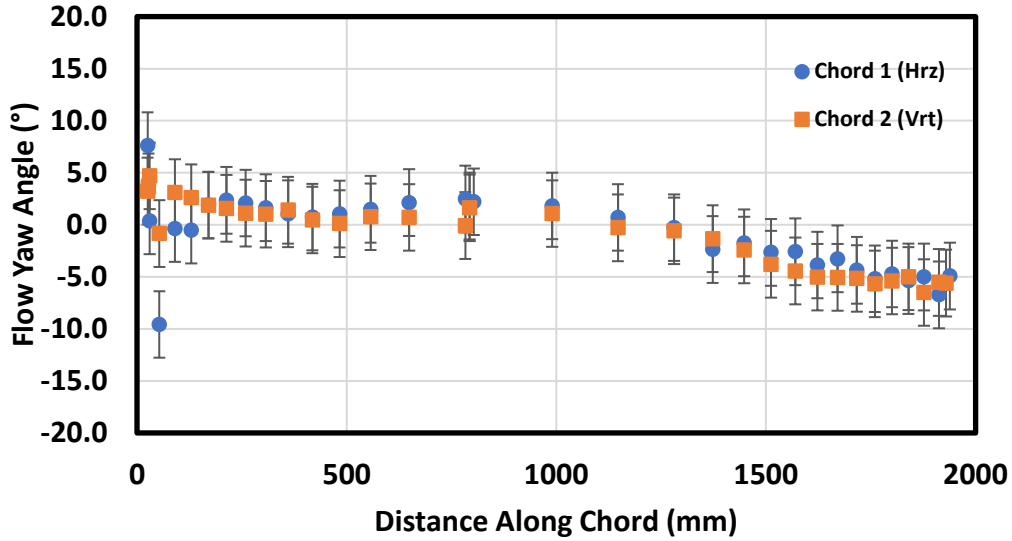
Fig. 15. Profiles of flow yaw angle for chords 1 and 2. Error bars represent the estimated expanded uncertainty for flow yaw angle, ±3.2°.
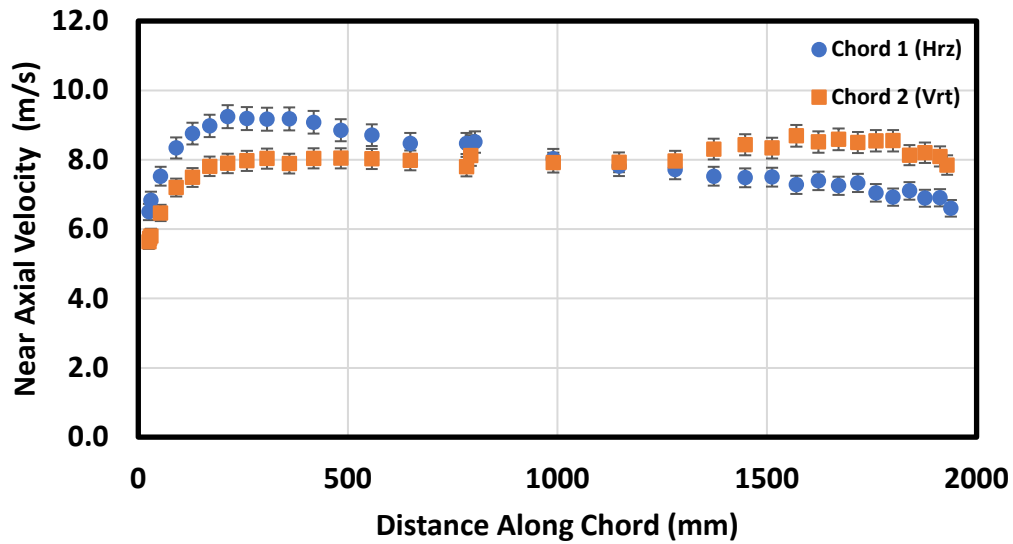
Fig. 16. Profiles of near axial velocity for chords 1 and 2. Error bars represent the estimated expanded uncertainty of near axial velocity, ±3.6 %.

Results of near axial velocity are shown in Fig. 16. The distribution of flow on chord 1 (horizontal) is skewed, with a maximum velocity of 9.2 m/s. The distribution on chord 2 (vertical) has more symmetry and is almost uniform across the central core. Maximum velocity on chord 2 is 8.7 m/s. The results provide evidence of skewed flow distributions that can lead to errors in exhaust flow measurements when the flow field is not adequately characterized. The reported value at each traverse position along the chord is the mean of at least 30 measurements. Relative standard uncertainty of the velocity measured at each position is estimated at ±1.4 % (See Appendix B, Table B.1). The contribution to uncertainty due to the fluctuating flow is represented as the standard deviation of the mean (SDOM) and is estimated at ±1.1 %. Adding the estimates in quadrature, the relative expanded uncertainty of the near axial velocity is estimated at ±3.6 % for this demonstration. As stated previously, the reported velocity is the mean of at least 30 measurements. The uncertainty due to flow fluctuations can be reduced by conducting more measurements at each traverse position. This will extend the time to conduct a flow characterization experiment, but it is an option to the user for controlling measurement uncertainty.

5.   Summary

Measurements of total flow are critical for quantifying emissions rates of greenhouse gases and pollutants from the smokestacks of fossil fuel combustion sources. Detailed characterizations of the flow are necessary to evaluate and improve the accuracy of continuous flow monitoring systems. This report has documented the design and performance of NFRL's own system of automated traverse probes for flow characterization. The system was designed to meet the objectives of the test methods developed by regulatory agencies and consensus standards organizations for the emissions industry. Where possible, automation of the procedures of the test methods has been implemented.

Field deployment of the system has been demonstrated with mounting the system at an NFRL exhaust duct to provide a preliminary characterization of the exhaust flow. The system will be utilized to conduct in-line calibrations of the flow monitoring devices installed at NFRL's exhaust ducts. This is a prototype for future designs of the system which can be applied to characterize flow conditions for similar-sized flue gas exhaust ducts and smokestacks. Further work to improve the system design for better operations and improved accuracy are on-going. Other potential uses of the system are precise positioning of probes (velocity, gas sampling, etc.) or instruments (thermocouples, heat flux sensors, etc.) in and around adverse environments such as enclosure fires or open burns.

References

[1]   Bryant R, Sanni O, Moore E, Bundy M, Johnson A (2014) An Uncertainty Analysis of Mean Flow Velocity Measurements Used to Quantify Emissions from Stationary Sources. *Journal of the Air & Waste Management Association* 64(6):679-689. https://doi.org/10.1080/10962247.2014.881437

[2]   Bundy M, Hamins A, Gross J, Grosshandler W, Choe L (2016) Structural Fire Experimental Capabilities at the NIST National Fire Research Laboratory. *Fire Technol* 52(4):959-966. https://doi.org/10.1007/s10694-015-0544-4

[3]   EPA (2007) Determination of Stack Gas Velocity and Volumetric Flow Rate with Two-Dimensional Probes. (Environmental Protection Agency, Washington, D.C.), EPA Method 2G, February 2007.

[4]   ASTM International (2006) Standard Test Method for Average Velocity in a Duct (Pitot Tube Method). ASTM D3154-00, May 2006.

[5]   ISO (1994) Stationary Source Emissions - Measurement of Velocity and Volume Flowrate of Gas Streams in Ducts. (International Organization for Standardization, Switzerland), ISO 10780:1994(E).

[6]   Traina JE (1995) Automated Flow Measuring Device. United States Patent Office 5394759 (March 1995).

[7]   Beaudin AB (1997) Automated Gas Measurement System. United States Patent Office 5635652 (June 1997).

[8]   Fleming MM, Devlin, BR, Gentry, MR (2009) Automated System and Method for Probe Measurement of Stack Gas Flow Properties. United States Patent Office 7624654 (December 2009).

[9]   EPA (2000) Determination of Stack Gas Velocity and Volumetric Flow Rate (Type S Pitot Tube). (Environmental Protection Agency, Washington, D.C.), EPA Method 2, February 2000.

[10]   Shinder II, Moldover MR, Filla BJ, Johnson AN, Khromchenko VB (2021) Facility for Calibrating Anemometers as a Function of Air Velocity Vector and Turbulence. *Metrologia* 58(4). https://doi.org/10.1088/1681-7575/ac0a92

[11]   Shinder II, Crowley CJ, Filla BJ, Moldover MR (2015) Improvements to NIST'S Air Speed Calibration Service. *Flow Measurement and Instrumentation* 44:19-26. https://doi.org/10.1016/j.flowmeasinst.2014.11.005

[12]   ISO (2008) Evaluation of Measurement Data - Guide to the Expression of Uncertainty in Measurement. (International Organization for Standardization, Switzerland), JCGM 100:2008.

Appendix A.   List of Symbols

C_{SP}
calibration constant for S-probe

D
inner diameter of exhaust duct or smokestack

d
traverse position across the exhaust duct or smokestack

M
molecular mass

P_s
static pressure

ΔP
differential pressure

T
temperature

u
standard uncertainty

U
expanded uncertainty (95 % confidence interval, k = 2.0)

V
gas velocity

Greek

ρ
gas density

σ
standard deviation (repeatability)

θ
rotational position of probe (angle relative to axis of exhaust duct or smokestack)

Subscripts

e
exhaust

y
yaw

Appendix B.   Uncertainty Budgets

Estimates of measurement uncertainty were evaluated using the approximate methods described in the ISO GUM. [12] Measurement processes that were based on input measurements, x_i, were modeled as an output quantity, y:

$$y = y(x_1, x_2, x_3, \ldots, x_N)$$ (B1)

In the case that all input quantities, x_i, are uncorrelated, the relative combined standard uncertainty is given by

$$\frac{u(y)}{y} = \sqrt{\sum_{i=1}^{N} \left(s_i \frac{u(x_i)}{x_i}\right)^2}$$ (B2)

Where $u(x_i)$ is the standard uncertainty for each input, and s_i is the associated dimensionless sensitivity coefficient given by

$$s_i = \frac{\partial y}{\partial x_i} \frac{x_i}{y}$$ (B3)

Equation (B2) provides the propagation of uncertainty from each instrument and input parameter into the measurement model, Eq. (B1). The relative expanded uncertainty is defined as:

$$\frac{U(y)}{y} = k \frac{u(y)}{y}$$ (B4)

Where $k = 2.0$, is the coverage factor for the 95 % confidence interval.

Table B.1 Estimated uncertainty budget for the near-axial velocity measurement.

Measurement / Parameter, x_i	Value	$u(x_i)/x_i$	s_i	% Contribution
C_{SP} (-)	0.825	0.013	1.0	92.3
θ_y (°)	1.8	0.889	-0.001	0.4
ΔP (Pa)	56.0	0.005	0.5	3.4
T (K)	290.7	0.005	0.5	3.4
P_s (Pa)	98 468	0.000 2	-0.5	0.0
M_e (kg /kmol)	28.97	0.0017	-0.5	0.4
R (J/kmol K)	8314.47	0.000 0	0.5	0.0
V_{SP} (m/s)	8.04	0.0135		Standard, *u(y)/y*
		0.027		Expanded, *U(y)/y*